Article:
ROBINSON, ALASTAIR, HILL-CASEY, FRASER, DUCKETT, Simon B. et al. (2026) Photochemical pump, benchtop NMR probe spectroscopy for reaction monitoring with parahydrogen. MAGNETIC RESONANCE IN CHEMISTRY. ISSN: 0749-1581

https://doi.org/10.1002/mrc.70124

ORIGINAL ARTICLE

Photochemical pump, benchtop NMR probe spectroscopy for reaction monitoring with *para*hydrogen

Alastair D. Robinson[1,2] | **Fraser Hill-Casey**[1,3] | **Simon B. Duckett**[1] | **Meghan E. Halse**[1]

[1]Department of Chemistry, University of York, York, UK, YO10 5DD

[2]Current address: Department of Chemical Engineering and Biochemistry, University of Cambridge, Cambridge, UK, CB3 0AS

[3]Current address: Gold Standard Phantoms Limited, Sheffield, UK

Correspondence
Department of Chemistry, University of York, York, UK, YO10 5DD
Email: meghan.halse@york.ac.uk; simon.duckett@york.ac.uk

Funding information
UK Engineering and Physical Sciences Research Council (EPSRC): EP/R028745/1 and EP/M020983/1

KEYWORDS
NMR spectroscopy, ^{1}H, *para*hydrogen, hyperpolarisation, photochemistry, reaction monitoring, iridium and ruthenium dihydrides

Abstract

The ability to observe transient intermediates and determine precise kinetic parameters is fundamental to understanding catalysis. This study demonstrates a methodology for the *in situ* investigation of photochemical ligand exchange and oxidative addition using a benchtop NMR spectrometer equipped with a through-bore UV irradiation system. To overcome the inherent sensitivity limitations of benchtop NMR, *para*hydrogen-induced polarisation (PHIP) was employed, providing significant signal enhancements for hydride-containing products. Specifically, the addition of pH$_2$ to *trans*-[IrCl(CO)(PPh$_3$)$_2$], that proceeds over 10 min, was monitored yielding a second-order rate constant, 1.36 ± 0.02 M^{-1} s^{-1}. To resolve faster catalytic processes, pump-probe synchronization between the UV pulse and NMR detection was implemented. A spin-lock pulse was also added to preserve the singlet state of the pH$_2$-derived hydride ligands in the reaction products, enabling the observation of coherent magnetic oscillations after reaction in the corresponding 2D pump-probe NMR spectra. Following optimisation on diagnostic zero-quantum correlations for *cis*-[Ru(H)$_2$(dppe)$_2$], a set of iodo-derivatives of Vaska's complex were explored. For these systems two photochemical pathways were effectively mapped, enabling the identification of several ligand-exchange products. These results

establish that the combination of hyperpolarisation and synchronized *in situ* irradiation makes benchtop NMR a powerful tool for the study of reactivity.

1 | INTRODUCTION

NMR is a powerful method to probe chemical systems in a non-invasive manner to obtain a wealth of information about structure, kinetic behaviour and associated reaction mechanisms.[1–3] Photochemical processes are of significant interest as they underpin many essential biological,[4,5] medicinal[6,7] and industrial applications.[8,9]

Photochemical processes can be monitored by NMR through either an *ex situ* or *in situ* approach.[10,11] The *ex situ* method, where the irradiation step occurs outside of the magnet, benefits from simplicity and affordability, but requires manual[12] or automated (such as through use of a flow loop)[13,14] transfer of the sample into the NMR spectrometer for detection. The *in situ* approach removes the transfer step and as such is favourable for observing fast processes. *In situ* methods fall into four main categories: through-bore, irradiation from below the sample,[15–18] through-probe, irradiation through the probe onto the side of the sample,[19–21] irradiation through an optical fibre inserted into the sample itself[22–25] and through using the NMR tube as a light guide (as demonstrated by Bramham *et al.* with NMRTorch).[26]

Benchtop NMR ($B_0 = 1-2$ T) reflects a more compact and cost-accessible alternative to standard high-field ($B_0 > 7$ T) NMR that has many advantages for reaction monitoring applications. The significantly reduced footprint of benchtop NMR, combined with properties such as external locking systems (enabling the use of protonated solvents)[27] and greater sample access, has been exploited to monitor reaction progress,[28,29] to gain mechanistic insights[30,31] and to determine key kinetic parameters.[32,33] Benchtop NMR is also well suited to *in situ* reaction monitoring, where the spectrometer is directly incorporated into a flow setup.[30,34–37] These same advantages apply to monitoring photochemical processes, where the integration of the irradiation step is greatly simplified by the compact size of benchtop NMR spectrometers. In addition, many models have an open bore, allowing easy access for *in situ* irradiation. Photochemical reaction monitoring using benchtop NMR has been demonstrated with both *ex situ*[38,39] and *in situ* irradiation, with integration of the light source either within the sample through fibre optics[40] or through bore using the NMR tube as a light guide.[26]

A challenge for the use of benchtop NMR for photochemical reaction monitoring is the reduced sensitivity associated with the moderate magnetic fields of benchtop NMR spectrometers. This can be overcome through the use of hyperpolarisation.[41] A range of hyperpolarisation methods have been developed that boost the sensitivity of NMR by generating large population differences across the nuclear spin states.[42] Here we focus on the *para*hydrogen-induced polarisation (PHIP) technique,[43–45] which uses $p\mathrm{H_2}$, the singlet nuclear spin isomer of $\mathrm{H_2}$, as the source of hyperpolarisation. PHIP is particularly advantageous for benchtop NMR applications because $p\mathrm{H_2}$ is relatively cheap, easy to prepare and generates hyperpolarised signals quickly (down to sub-second timescales).[46]

*Para*hydrogen is NMR silent. For PHIP to occur, the symmetry of $p\mathrm{H_2}$ must be broken, for example by a chemical reaction. Once the symmetry of the $p\mathrm{H_2}$-derived protons in the product molecule is broken, via magnetic or chemical inequivalence, the NMR-silent singlet state will evolve into observable hyperpolarisation through selective overpopulation of nuclear spin states.[47,48] In standard PHIP experiments, hyperpolarised product is built-up over a period of seconds. While beneficial to ensure a strong hyperpolarised response, some of the potential insights about the mechanism of $p\mathrm{H_2}$ addition are lost due to the time-averaged nature of the NMR response.[48] An alternate approach is to use photochemical initiation of the reaction with $p\mathrm{H_2}$ to generate a synchronised starting point in order to observe the coherent evolution of the system.

Photochemical initiation has been used across several hyperpolarisation methods previously. Chemically-induced dynamic polarisation (CIDNP), which relies on a radical-pair mechanism to generate hyperpolarisation, was combined with photochemical initiation in 1978 for the study of proteins[49] and has been applied to biopolymers,[50] ketone flash photolysis[51] and high-throughput fragment screening.[52] Fragment screening using photo-CIDNP has also been demonstrated with benchtop NMR detection, where significantly higher signal enhancements were observed in the lower field of the benchtop NMR.[53] Photo initiation has also been combined with *para*hydrogen-based hyperpolarisation techniques, including both hydrogenative PHIP[25,54–56] and the signal amplification by reversible exchange (SABRE) method, where hyperpolarisation is generated catalytically without chemically altering the target molecule.[57] Of particular interest here is the photochemical pump - NMR probe approach that

was first demonstrated in 2014 on a 600 MHz spectrometer coupled to an Nd:YAG laser.[55] The pump-probe experiment consists of an initial laser pulse, followed after a fixed τ delay by NMR detection. Through variation of τ, the evolution of the system can be observed over timescales from microseconds to seconds. This experiment has been used to follow pH$_2$ addition reactions, such as the addition of pH$_2$ to *trans*-[IrI(CO)(PPh$_3$)$_2$][58] and [Ru(H)$_2$(CO)(PPh$_3$)$_3$].[59] It also enables the observation of micro-to-millisecond evolution of magnetic coherences following pH$_2$ addition. These coherent oscillations give insight into the spin-system of the products formed and the mechanism of the pH$_2$ addition step.[60]

Here we present an *in situ* photochemical setup for PHIP-enhanced benchtop NMR spectroscopy. The photochemically-initiated addition of pH$_2$ to *trans*-[IrCl(CO)(PPh$_3$)$_2$] is monitored, kinetic parameters are extracted and compared to previous studies using thermally initiated pH$_2$ addition. To monitor faster processes, a photochemical pump - NMR probe methodology is developed, where a relay device enables computer-controlled synchronisation of the UV irradiation and NMR detection steps. The pump-probe method is used to observe the evolution of magnetic coherences over millisecond timescales following pH$_2$ addition to *cis*–[Ru(H)$_2$(dppe)$_2$] and *trans*-[IrI(CO)(PPh$_3$)$_2$] , providing insights into the pH$_2$ addition mechanisms and the formation of low concentration photoproducts.

2 | EXPERIMENTAL

2.1 | Samples and Synthesis

The structures of the metal dihydride complexes explored within this paper are given in Figure 1.

The synthesis for *trans*-[IrCl(CO)(PPh$_3$)$_2$] is given in a previous study by Robinson *et al.*[61] following a procedure designed by Chock *et al.*[62] Upon addition of H$_2$, [IrCl(H)$_2$(CO)(PPh$_3$)$_2$] (**1**) is formed. Select NMR characterisation for this hydride complex is as follows: ^{1}H NMR (400 MHz, C$_6$D$_6$) δ: 7.91 (m, 12H, o-Ph), 7.02 (m, 12H, m-Ph), 6.96 (m, 6H, p-Ph), -6.70 (td, 1H, J_{HP} = 17.6 Hz, J_{HH} = 4.6 Hz), -17.49 (td, 1H, J_{HP} = 13.9 Hz, J_{HH} = 4.6 Hz) . ^{31}P{^{1}H} NMR (162 MHz, C$_6$D$_6$) δ: 9.9.

trans-[IrI(CO)(PPh$_3$)$_2$] was synthesised following the procedure established by Chock *et al.*[62] A round-bottom flask was charged with *trans*-[IrCl(CO)(PPh$_3$)$_2$] (102 mg, 0.13 mmol) dissolved in C$_6$H$_6$ (10 mL) to which NaI (215 mg, 1.43 mmol) in ethanol (5mL) was added under an N$_2$ atmosphere. The mixture was stirred in darkness (1 hr), after which a crude product was obtained. The residue was dissolved in a benzene-water mixture (75:25, v/v, 13 mL), from which the organic layer was dried *in vacuo* to obtain the final product (73 mg, 65%). ^{1}H NMR (400 MHz, C$_6$D$_6$) δ: 7.96 (m, 12H, o-Ph), 7.01 (m, 18H, m-Ph and p-pH). ^{31}P{^{1}H} NMR (162 MHz, C$_6$D$_6$) δ: 20.7. IR (ATR, cm^{-1}): 1992 (ν_{CO}).

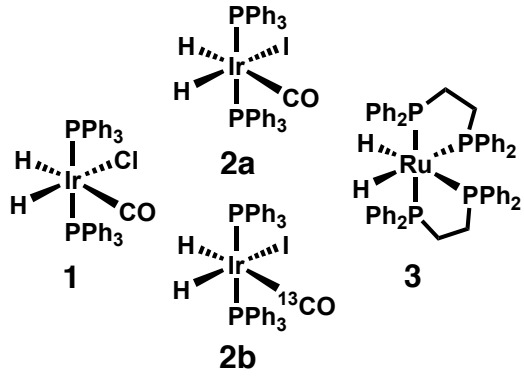

FIGURE 1 Structures of complexes used within this study.

Upon addition of H$_2$, [Ir(H)$_2$(I)(CO)(PPh$_3$)$_2$] **(2a)** was formed. ^{1}H NMR (400 MHz, C$_6$D$_6$) δ: 7.89 (m, 12H, *o*-Ph), 7.02 (m, 12H, *m*-Ph), 6.95 (m, 6H, *p*-Ph), -8.49 (td, 1H, J_{HP} = 17.4 Hz, J_{HH} = 4.2 Hz), -14.90 (td, 1H, J_{HP} = 13.7 Hz, J_{HH} = 4.2 Hz). ^{31}P{^{1}H} NMR (162 MHz, C$_6$D$_6$) δ: 5.4.

The preparation of *trans*-[IrI(^{13}CO)(PPh$_3$)$_2$] was performed in two stages using procedures modified from Burk *et al.*[63] and Chock *et al.*[62] [IrCl(COD)]$_2$ (100 mg, 0.15 mmol) and PPh$_3$ (165 mg, 0.63 mmol) were dissolved in a hexane/DCM mixture (50:50 v/v, 20 mL) under an N$_2$ atmosphere. After stirring (10 min), the solution was placed under a static pressure of ^{13}CO (1 atm) and stirred (1 hr). The solution was concentrated, and the precipitate formed was washed with hexane (3 x 10 mL) and dried *in vacuo* to give *trans*-[IrCl(^{13}CO)(PPh$_3$)$_2$] (149 mg, 64%). Under an N$_2$ atmosphere, *trans*-[IrCl(^{13}CO)(PPh$_3$)$_2$] (100 mg, 0.13 mmol) was dissolved in C$_6$H$_6$ (15 mL) and charged with NaI (199 mg, 1.33 mmol) in ethanol (6 mL). Following stirring (1 hr), the suspension was concentrated and the precipitate formed was dissolved in a benzene-water mixture (75:25 v/v, 13 mL). The organic layer was separated and dried *in vacuo* to give a pale yellow powder (86 mg, 76%). ^{1}H NMR (400 MHz, C$_6$D$_6$) δ: 7.96 (m, 12H, *o*-Ph), 7.01 (m, 18H, *m*-Ph and *p*-pH). ^{31}P{^{1}H} NMR (162 MHz, C$_6$D$_6$) δ: 20.7. IR (ATR, cm^{-1}): 1942 (ν_{CO}).

Upon addition of H$_2$, [Ir(H)$_2$(I)(^{13}CO)(PPh$_3$)$_2$] (**2b**) is

formed. ^{1}H NMR (400 MHz, C_6D_6) δ: 7.89 (m, 12H, *o*-Ph), 7.02 (m, 12H, *m*-Ph), 6.95 (m, 6H, *p*-Ph), -8.49 (dtd, 1H, J_{HC} = 42.5 Hz, J_{HP} = 17.4 Hz, J_{HH} = 4.2 Hz), -14.90 (tdd, 1H, J_{HP} = 13.7 Hz, J_{HH} = 4.2 Hz, J_{HC} = 2.3 Hz). ^{31}P{^{1}H} NMR (162 MHz, C_6D_6) δ: 5.4.

The *cis*–[Ru(H)$_2$(dppe)$_2$] (**3**) complex used within this study was synthesised previously,[60] following a literature procedure developed by Nolan *et al.*[64] This pathway is non-regioselective forming a mixture of *trans* and *cis* isomers. *trans*–[Ru(H)$_2$(dppe)$_2$] is not pH$_2$ active because the hydride ligands are both chemically and magnetically equivalent. Therefore hyperpolarisation is only observed for *cis*–[Ru(H)$_2$(dppe)$_2$]. Select characterisation for *cis*–[Ru(H)$_2$(dppe)$_2$] is as follows: ^{1}H NMR (400 MHz, C_6D_6) δ: -8.33 (m, 2H). ^{31}P{^{1}H} NMR (162 MHz, C_6D_6) δ: 79.5 (t, 2P, J_{PP} = 16 Hz), 65.5 (t, 2P, J_{PP} = 16 Hz).

All reaction solvents and benzene-d_6 (for NMR sample preparation) were purchased from Sigma-Aldrich. Reagents for the synthesis of *trans*-[IrI(CO)(PPh$_3$)$_2$] and its derivatives were purchased from Precious Metals Online (iridium(III) chloride 3-hydrate), Fissons (sodium iodide) or synthesised by other members of the research group ([IrCl(COD)]$_2$).

2.2 | NMR magnet and hyperpolarisation studies

All experiments were conducted on a 1 T (43 MHz) Spinsolve Carbon (Magritek, Germany) at 301.5 K. Prior to any NMR experiments, the spectrometer was locked, shimmed to a full-width-half-maximum of < 0.5 Hz and the spectrometer frequency was calibrated using a reference sample of 10:90 (v/v) H_2O:D_2O.

For all PHIP samples, the required mass of analyte was weighed and transferred in an N_2 glovebox. A bulk solution in C_6D_6 was prepared to the desired concentration, with 0.6 mL aliquots dispensed into J Young tap NMR tubes using glass Luer-lock syringes. Samples were then degassed using three freeze-pump-thaw cycles[65] on a high-vacuum line. pH$_2$ was generated using an in-house rig (previously detailed by Richardson *et al.*[66]) with a >98% purity. pH$_2$ was added to the head-space of the NMR tube at a fixed pressure of (4.0 $\pm$ 0.1) bar, verified using a MKS Baratron pressure gauge. Manual shaking was used to introduce pH$_2$ into solution prior to each hyperpolarisation experiment.

Replenishment of pH$_2$ in the headspace of the NMR tube between each acquisition adds significant experiment time (with each refill taking at least 1 minute) and can lead to issues such as solvent evaporation due to the repeated exposure of the liquid state sample to a vacuum. Here it was found that four repeats of the experiment, with sample shaking in between each acquisition, could be performed before a threshold deviation of >5% signal loss was exceeded (see Figure S5c in the supporting information). Unless otherwise stated, for all hyperpolarisation studies the NMR sample was shaken after every step with pH$_2$ being replenished every four steps. Furthermore, the increments of the pseudo-2D experiments were performed in a randomised order to minimise the impact of solvent evaporation on the collected datasets.

2.3 | Irradiation source and photochemistry

The UV source used was a Bluewave 75 Spot Curing Lamp (Dymax Europe GmbH, Wiesbaden, Germany). This is a 75 W short-arc bulb that emits strong UV irradiation within the 300 - 450 nm wavelength range. The lamp used was measured to deliver a maximum output of 4.05 W (density of 515 W cm^{-2}) with an ability to linearly vary the output down to 0.10 W. The Bluewave 75 lamp was coupled to a liquid light guide (containing an optically transparent liquid in the 270 to 720 nm range) with quartz glass termini on either side. As standard, the lamp is operated manually using either a foot pedal or through use of an internal timer. The liquid light guide was held in place within the spectrometer just below the bottom of the NMR tube by a 3D printed PLA insert. Locking, tuning and shimming are performed once the setup is within the spectrometer.

For automation of the UV irradiation, a microcontroller relay assembly was constructed from an Arduino Nano and a mechanical SPDT (Single Point Double Throw) relay module. A schematic of this setup is given in Figure 2b. The relay device enables a low voltage trigger signal to directly operate the shutter on the UV lamp. Two modes of operation have been coded into the microcontroller, allowing for either independent on/off commands to be given or the opening of the shutter for a user allotted duration. Additional details about the device and code are provided within the Supporting Information. To ensure safe operation, an internal timer within the Arduino will close the shutter after 30 s if no command to close the shutter is sent.

Unless otherwise specified in the text, pump-probe photochemistry experiments were performed with a 0.5 s irradiation period. This was selected as a compromise to generate a sufficient population of the unreacted precursor while preventing over-consumption of pH$_2$, which would lead to lower levels of hyperpolarisa-

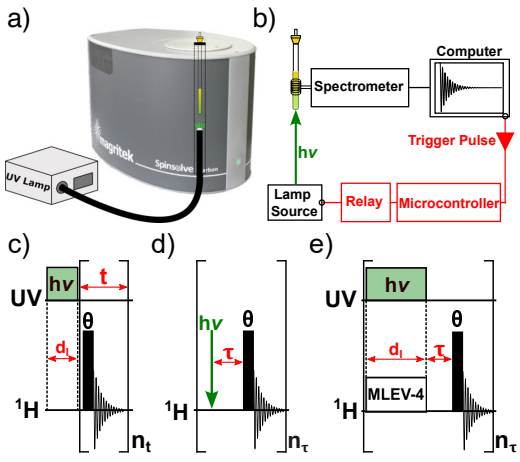

FIGURE 2 (a) Cartoon representation and (b) schematics for the through-bore *in situ* photochemical setup alongside pulse sequences for (b) low-field photochemical reaction monitoring, (c) high-field laser initiated pump-probe experiments and (d) low-field lamp initiated pump-pump experiments.

tion (discussed in the Supporting Information, Section S3).

3 | RESULTS AND DISCUSSION

3.1 | Developing an *in situ* photochemistry setup

The benchtop NMR setup for *in situ* photo-initiated PHIP hyperpolarisation is illustrated in Figure 2a. The setup uses a broadband UV light source that can be operated either manually, using a foot pedal, or through use of an internal timer allowing fixed durations of irradiation between 0.01 and 99.99 s. In this work, we irradiate by placing an optical fibre just below the NMR detection region to minimise the path length between the fibre and the NMR tube. This does not require any modification to the NMR tube, as would be the case when placing the optical fibre within the NMR sample, making the overall system inexpensive and compact.

3.2 | Photochemical reaction monitoring

Previously, we presented a method for pH_2-enhanced reaction monitoring using benchtop NMR detection and applied it to the addition of pH_2 to Vaska's complex (*trans*-[IrCl(CO)(PPh_3)$_2$]) to form [IrCl(H)$_2$(CO)(PPh_3)$_2$] (**1**).[61] In this method, pH_2 was added to the headspace of a sample containing Vaska's complex, which was shaken and placed into the NMR spectrometer. The progress of the reaction was monitored via the decay of the hyperpolarised hydride peaks. The *in situ* photochemical setup allows for this reaction monitoring approach to be combined with a photoinitiation step. First, [IrCl(H)$_2$(CO)(PPh_3)$_2$] is irradiated *in situ* to generate the precursor, Vaska's complex, within the sample (the first step in Figure 3a). When the sample is charged with fresh pH_2, the generated Vaska's complex will react with pH_2 to reform [IrCl(H)$_2$(CO)(PPh_3)$_2$] with hyperpolarised hydrides (the second step in Figure 3a). An average SNR of 68 was observed for the initial hydride ligand signals recorded for the [IrCl(H)$_2$(CO)(PPh_3)$_2$] complex.

For this study, samples of Vaska's complex (0.43 mM) were first placed under pH_2 and allowed to fully convert to **1**. Subsequently, fresh pH_2 was added, the sample was shaken, placed into the spectrometer and left to equilibrate to the temperature of the spectrometer (301.5 K) for 10 minutes. Following equilibration, the sample was UV-irradiated for 10 s (initiated via foot pedal) and then monitored using the ^{1}H NMR pulse sequence in Figure 2c, where the pulse angle was set to 45° and a spectrum was recorded every 5 s for 128 steps (giving a total acquisition time of 10.7 min). The generated pseudo-2D dataset was analysed through integration and accumulation of the pH_2-enhanced hydride signals, as described previously,[61] allowing for the determination of an average rate constant for the reaction of $k_2 = 1.36 \pm 0.02 M^{-1}s^{-1}$ over five repeat experiments (Figure 3b, red). The blue trace in Figure 3b is the accumulated hyperpolarised hydride signal obtained without photo initiation, reproduced from Reference [[61]], with corresponding reaction rate $k_2 = 0.89 \pm 0.02\ M^{-1}s^{-1}$.

The rate of H_2 addition to *trans*-[IrCl(CO)(PPh_3)$_2$] is known to have a temperature dependence of 0.06 $M^{-1}s^{-1}K^{-1}$.[61,67] Therefore compared to the literature k_2 value of 0.86 $M^{-1}s^{-1}$ at 301. 5 K,[67] the k_2 rate measured using photo-initiation implies sample heating of ΔT = 8.4 K during the 10 s UV-irradiation period. This is consistent with the observed temperature change of ΔT = 8.7 K for a 0.6 mL sample of water, measured following 10 s of *in situ* UV-irradiation by a thermocouple introduced into the NMR tube (data given in Section S1 of the Supporting Information).

One advantage of photochemical initiation is that the sample can be situated within the spectrometer when the reaction starts, whereas thermal initiation involves the manual transfer of the sample into the spectrometer following shaking. This allows for faster pro-

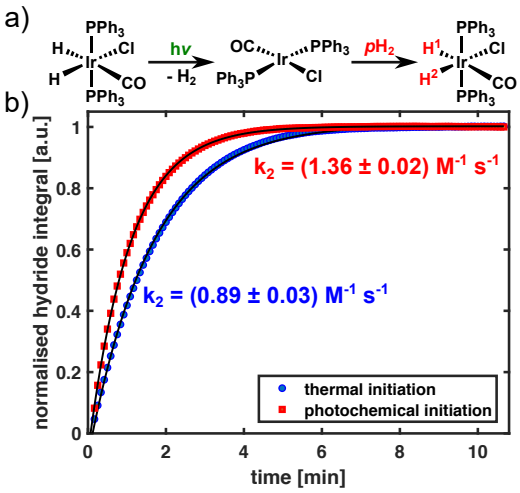

FIGURE 3 (a) Reaction scheme for photochemically initiated addition of pH_2 to *trans*-[IrCl(CO)(PPh_3)$_2$] and (b) comparison between the average rate of reaction measured when using thermal or photochemical initiation. Thermal reaction monitoring data has been previously published as part of Reference [[61]].

cesses to be examined. To highlight this, the addition of pH_2 to the iodo-derivative of Vaska's complex, *trans*-[IrI(CO)(PPh_3)$_2$], was interrogated (Figure 4a). Previous monitoring of this system by Procacci *et al.* gave a k_2 rate constant of 326 $M^{-1}s^{-1}$ at 298 K, with the reaction reaching completion within a 5 s window.[58] To explore this system, a sample of [Ir(H)$_2$(I)(CO)(PPh_3)$_2$] (0.38 mM) was prepared using the procedure described above and irradiated for 1 s prior to NMR acquisition. NMR acquisition was performed in 1 s increments, allowing for five spectra to be obtained over the course of the reaction, as shown in Figure 4b.

From the collected dataset, the reaction was seen to go to completion over a period of 5 s with a maximum SNR of 14 observed for the initial timestep. However, the time resolution of the measurement, which is limited by the time required to acquire each NMR spectrum, is insufficient to determine quantitative kinetic parameters for this reaction. Similarly to the study performed with **1**, heating of the NMR sample was observed, which is expected to further increase the rate relative to that measured at 298 K. In order to investigate system evolution over shorter timescales, it is necessary to move away from a continuous reaction monitoring approach to a pump-probe method that provides access to evolution over millisecond to second timescales.

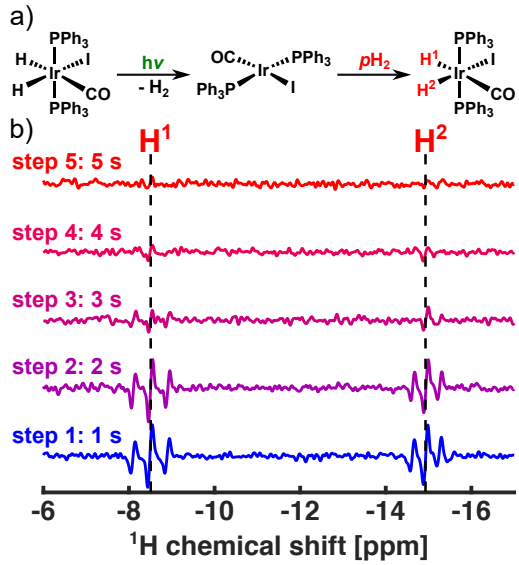

FIGURE 4 (a) Reaction scheme for photochemically initiated addition of pH_2 to *trans*-[IrI(CO)(PPh_3)$_2$] and (b) pH_2-enhanced ^{1}H benchtop NMR spectra of the degenerate reaction in (a) as a function of time following 1s of *in situ* UV irradiation.

3.3 | Development of a photochemical pump - benchtop NMR probe method

To implement the pump-probe approach on the benchtop NMR spectrometer, a manual foot trigger is not suitable because the photo-irradiation and NMR acquisition steps must occur with precise timing. Hence, a microcontroller relay assembly was implemented to facilitate communication between Prospa (the programming language of the Magritek Spinsolve spectrometer) and the shutter on the Bluewave lamp source, allowing for synchronisation between the photochemical pump and NMR probe steps. A schematic of this setup is given as Figure 2b.

With this fully integrated shutter control, pump-probe NMR spectroscopy can now be performed. However, two changes had to be made to the previously published high-field pump-probe pulse sequence (Figure 2d) when using a continuous wave light source with benchtop NMR detection. Firstly, the irradiation time, d_I, is now a non-negligible feature of the experiment as periods on the millisecond to second timescale are required to build up a suitable concentration of species for benchtop NMR detection. Consequently, a synchronous starting point for observing short-lived coher-

ences is no longer achieved. This limitation was overcome by adding a spin-lock during UV irradiation as shown in Figure 2e. This procedure maintains a pseudo-singlet state in the product until decoupling is stopped - thus providing a synchronous starting point for magnetic evolution.[68,69]

An MLEV-4 decoupling cycle using four composite 180° inversion pulses was utilised for decoupling during irradiation.[70,71] Each MLEV-4 cycle has a duration of 2 ms with each composite pulse spaced by 0.5 ms to give an overall duty cycle of 7.5%. The number of MLEV-4 cycles required is calculated by dividing d_I by 2 ms and rounding to the nearest integer. This means irradiation of the sample will finish before decoupling ends, ensuring a synchronous starting point for the system.

3.4 | Pump-probe experiments on *cis*–[Ru(H)$_2$(dppe)$_2$]

Initial optimisation of the automated trigger was performed using an optically dilute sample of *cis*–[Ru(H)$_2$(dppe)$_2$] (**3**) (1.4 mg, 2.6 mM). The reaction being monitored, given in Figure 5a, is initiated by photochemical loss of H_2, which allows for a molecule of pH_2 to react with the unsaturated Ru centre that is generated. Oxidative addition of pH_2 to reform **3** breaks the symmetry of the pH_2-derived hydride ligands and generates observable hyperpolarisation after a suitable evolution period. The break in symmetry arises from the magnetic inequivalence of the hydride ligands in **3** due to the difference in *trans* and *cis* hydride-^{31}P couplings (ΔJ = 84 ± 1 Hz, Figure 5b).[55,60]

In order to compare the efficiencies of the computer-controlled shutter operation and the manual trigger, two single-scan hyperpolarisation experiments were performed. Prior to each measurement, the head-space of the NMR tube was charged with 4 bar of pH_2 and the tube was shaken to mix fresh pH_2 into solution. Figure 5b presents the spectra obtained for the manual (black) and automated (red) approaches.

While strong hyperpolarisation (SNR = 273) is evident when using the automated trigger (red), when using the manual technique, no hyperpolarised hydride ligand signals are observed (black). This can be explained by relaxation of the hyperpolarised signals during the delay between stopping irradiation and starting the NMR detection in the manual case. This hypothesis was confirmed by carrying out a series of variable delay experiments with the automated trigger. The hyperpolarised signals of **3** were found to decay with a hyperpolarised T_1 value of (250±30) ms such that no hyperpolarised signals are observed after 0.8 s (Figure S6 in the Supporting Information).

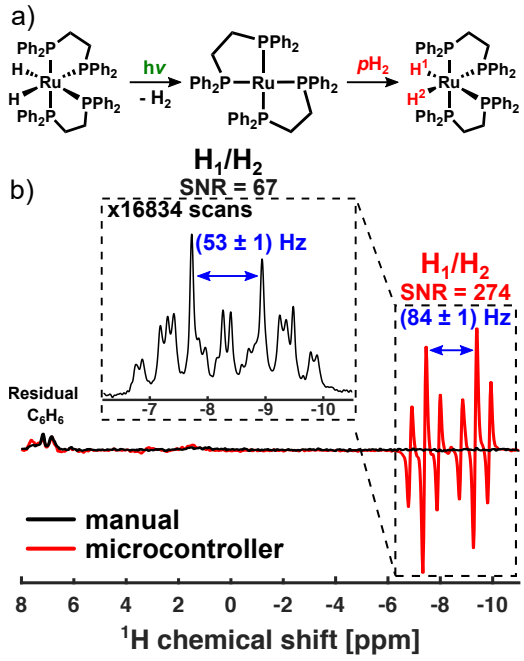

FIGURE 5 (a) Degenerate reaction scheme for the addition of pH_2 to *cis*–[Ru(H)$_2$(dppe)$_2$] (2.6 mM). (b) ^{1}H benchtop NMR spectra of **3** with *in situ* irradiation (d_I = 0.5 s, 1 scan) using the manual (black) and automated (red) initiation and an inset thermally-polarised spectrum recorded without irradiation (16384 scans, 14 hours).

The level signal enhancement achieved with the automated trigger set-up can be estimated by comparing the SNR of the hyperpolarised spectrum (red) with that for a reference non-hyperpolarised spectrum (inset, 16384 scans). Taking the number of scans into account, pH_2 hyperpolarisation provides a 530-fold increase in SNR. This large enhancement factor is essential to enable the signals of interest for this study to be observed in a single scan and with the required temporal resolution.

To test the influence of the spin-lock on the observed NMR signal over short timescales, a sample of **3** (1.8 mg, 3.3 mM) was irradiated and NMR signals measured between τ = 0 to 10 ms. Figure 6a shows the measured hydride signal without (left) and with (right) a spin-lock at select τ values. From these spectra, it is clear that the presence of the spin-lock leads to detectable signal oscillations on the ms timescale, indicating that the mag-

netic coherences are preserved during UV irradiation. A full pump-probe spectrum for pH_2 addition to **3** was obtained by extending the pump-probe time to τ = 126 ms (in 64 steps) and applying a Fourier Transform in the indirect dimension (Figure 6c). In this spectrum, the indirect dimension defines zero-quantum evolution during the pump-probe delay. Correlations are observed at $\Delta\nu = \pm(85 \pm 6)$ Hz, which matches the difference between the *trans* and *cis* hydride-^{31}P coupling in **3**. A more precise oscillation frequency of 84.11±0.05 Hz was obtained by selectively integrating the anti-phase peaks, as described previously,[60] and fitting the integrals as a function of the pump-probe delay to a decaying sine oscillation (Figure 6b).

The pump-probe spectrum of **3** acquired on the benchtop NMR spectrometer (43 MHz) is expected to be directly comparable to the corresponding high-field spectrum acquired at 600 MHz[55] because the zero-quantum evolution of the pH_2-derived singlet state is driven by differences in J coupling, which are field independent. However, the benchtop NMR pump-probe spectrum contains a strong component at 0 Hz. This feature is predicted by the theory to be due to strong coupling between the hydride ligands and has been observed previously in ^{31}P pump-probe spectra of **3** at high field, but with much lower intensity.[60] The high relative intensity of the 0 Hz peaks is likely here to reflect imperfect preservation of the pH_2 singlet state during the 0.5 s irradiation pulse. If some evolution of the singlet state does occur during irradiation, the correlations that oscillate at $\Delta\nu = \pm(85 \pm 6)$ Hz will experience destructive interference due to complexes that are formed in solution through time incoherent pH_2 addition. However, terms that do not oscillate (and therefore appear at 0 Hz in the pump-probe spectrum) accumulate constructively during this time.

3.5 | Photochemical pump - NMR probe spectroscopy of $[Ir(H)_2(I)(CO)(PPh_3)_2]$ and $[Ir(H)_2(I)(^{13}CO)(PPh_3)_2]$

For chemical systems where the pH_2-derived hydrides are chemically inequivalent, the zero-quantum oscillation frequencies during the pump-probe delay will be dictated by their difference in chemical shift,[60] which is field dependent. A benefit of benchtop NMR detection for chemical systems that have otherwise large chemical shift differences is that a narrower spectral width in the indirect dimension is required, which can be exploited for higher spectral resolution or shorter

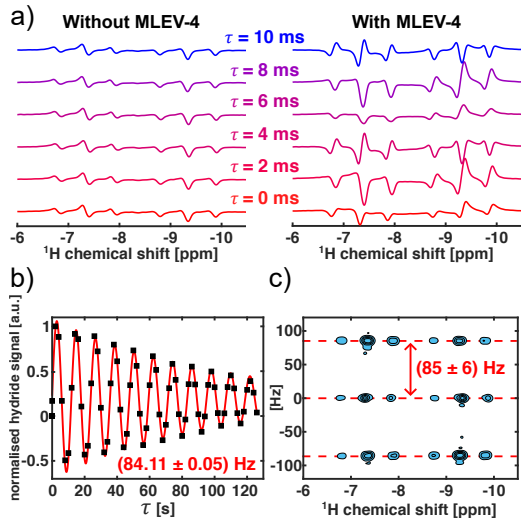

FIGURE 6 (a) Comparison between ^{1}H spectra collected for *cis*-[Ru(H)$_2$(dppe)$_2$] without and with MLEV-4 decoupling during irradiation using d_I = 0.5, τ = 0 - 10 ms and θ = 90°. (b) 1D oscillation and (c) 2D spectrum following a variable delay pump-probe experiment. Pump-probe data for *cis*-[Ru(H)$_2$(dppe)$_2$] (3.3 mM) was collected in 64 steps using θ = 90°, d_I = 0.5 s and τ delays between 0 and 0.126 s.

experiment times. To exemplify this, the pump-probe method was used to examine the addition of pH_2 to $[Ir(H)_2(I)(CO)(PPh_3)_2]$ (**2a**) and $[Ir(H)_2(I)(^{13}CO)(PPh_3)_2]$ (**2b**).

The hydride ligands in **2a** form part of an AX-type spin system and so the symmetry breaking feature during PHIP addition will be chemical inequivalence. With a chemical shift difference of 6.5 ppm between the two hydride multiplets, an oscillation frequency of $\delta\nu_{AX}$ = ±282 Hz is expected at 43 MHz. This corresponds to a 3.5 ms period of oscillation. In contrast, the hydride ligands in **2b** form part of an AXY-type spin system (where A and X are the chemically inequivalent hydride ligands that couple differently to the ^{13}C nucleus, Y). Now the peaks appear at $\pm\delta\nu_{AX}$ due to the chemical shift difference of the hydride ligands being further split into a doublet, with the splitting dictated by the difference between the *trans* and *cis* couplings to the Y nucleus ($\Delta J = J_{AY} - J_{XY}$). Using reference measurements taken at 400 MHz (to resolve the small cis J_{HC} coupling), the J coupling constants to the ^{13}CO nuclei for the two hydride resonances are $J_{HCtrans}$ = ±43 Hz (for H^1) and J_{HCcis} = ∓2 Hz (for H^2). These values give a ΔJ value

of 45 Hz and so the peaks for this system would be expected to appear at frequencies of ±260 Hz and ±305 Hz.

This study was performed on samples of 3.1 mM of **2a** and **2b** using a 1 s irradiation period (optimised for maximum signal with SNRs of 1096 and 602 achieved, respectively). A 64 step pump-probe experiment was performed with τ delays between 0 and 31 ms, with pH$_2$ refreshment every 4 steps. As there is potential for the sample to begin to degrade upon continued exposure to broadband UV light, randomisation of the time points was used to ensure sample degradation did not impact the observed oscillations.[58] The 2D pump-probe spectra of **2a** and **2b** are presented in Figure 7a and b, respectively.

The 2D pump-probe spectrum for **2a** (Figure 7a) exhibits zero-quantum peaks at a $\Delta\nu$ value of $\pm(283 \pm 12)$ Hz (measured as (280.9 ± 1.2) Hz in the 1D oscillation), which agrees well with the evolution frequency of 282 Hz. For **2b** (Figure 7b), an additional 50 Hz splitting is observed in the indirect dimension due to the difference in coupling between the hydride ligands and the ^{13}C nucleus, as expected (a more accurate value of 45.3±1.4 Hz is obtained from the 1D oscillation frequencies of 303.0 ± 0.06 and 257.7 ± 0.08 Hz). Strong peaks are observed in both spectra at 0 Hz. As discussed above, these likely result from to a combination of strong coupling effects and the accumulation of non-oscillating terms during the irradiation period.

In addition to the hydride ligands of **2a** and **2b**, weaker hyperpolarised hydride ligand resonances are observed at δ -9.8, -12.6, -17.6 and -21.5 in this sample. Increasing the contour levels within the dashed boxes of the pump-probe spectra in Figure 7 by a factor of 10 reveals additional zero-quantum correlations for the peaks at δ -9.8, -12.6, and -17.6. The pattern of these zero-quantum oscillations reveal the presence of a *trans* hydride-phosphine coupling of ca. 140 Hz. We assign these peaks to the *tris*-phosphine complex, [Ir(H)$_2$(I)(PPh$_3$)$_3$], which was characterised previously as **3*** in Reference [[58]]. This species is formed due to light induced ligand exchange of CO for PPh$_3$. The absence of CO in this species is confirmed by the observation that its zero-quantum correlations have the same appearance in the presence and absence of ^{13}C (Figures 7a and b). The additional hydride species at -21.5 is an iridium dimer, previously observed in pump-probe experiments on **2a** at 600 MHz at elevated temperatures and following multiple laser shots.[58] The second hydride ligand peak for the dimer is expected at δ -18.6 and is therefore obscured by overlap with H^4 of [Ir(H)$_2$(I)(PPh$_3$)$_3$]. Interestingly, the hyperpolarised resonance of the dimer species does not evolve during the pump-probe delay, exhibiting a relatively consistent hyperpolarisation level over pump-pump delays from milliseconds to seconds. This suggests that it exchanges pH$_2$ thermally and therefore its hyperpolarisation is refreshed asynchronously throughout the pump-probe delay from the reservoir of pH$_2$ in solution. The observation of these very low concentration photoproducts and their behaviour over millisecond timescales on the benchtop NMR spectrometer is due to the remarkable signal amplification provided by pH$_2$ and the synchronisation of the photochemical irradiation and NMR detection steps.

4 | CONCLUSIONS

We have demonstrated detection of photochemically-induced *para*hydrogen-hyperpolarisation on a benchtop (1 T) NMR spectrometer. An *in situ* through-bore irradiation setup, using a broadband UV source, was implemented allowing for UV irradiation and NMR detection to occur without the need for manual sample transfer. The system was used to monitor the addition of pH$_2$ to Vaska's complex following irradiation of [IrCl(H)$_2$(CO)(PPh$_3$)$_2$]. The obtained rate constant, k_2 = 1.36±0.02 M^{-1}s^{-1}, indicates non-negligible sample heating occurred during the 10 s UV irradiation period. To explore the potential for the method to examine a faster thermal H$_2$ addition step, *trans*-[IrI(CO)(PPh$_3$)$_2$] was selected. Upon examination with pH$_2$, diagnostic signals were observed for [Ir(H)$_2$(I)(CO)(PPh$_3$)$_2$], mapping the pH$_2$ addition step over a 5 s window. However, only five time points could be sampled using the continuous monitoring approach, where NMR spectra were acquired sequentially following a single UV irradiation period. This time resolution failed to adequately define the signal growth curve required to determine an accurate rate constant.

To monitor chemical and magnetic evolution on shorter timescales, a photochemical pump - NMR probe method was implemented. Synchronisation between the UV irradiation and NMR detection was achieved using a microcontroller relay and software controls embedded into the NMR pulse sequence macro. A synchronous starting point for magnetic evolution during the pump-probe delay was achieved by applying a spin lock during the UV irradiation period.

The ability of this pump-probe approach to observe evolution on millisecond to second timescales was exemplified by the hyperpolarisa-

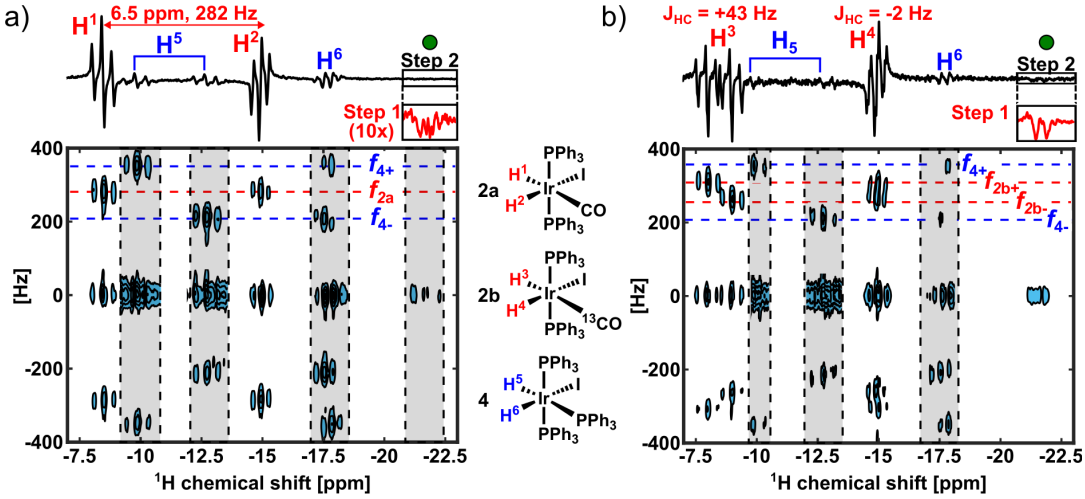

FIGURE 7 ^{1}H pump-probe spectra acquired at 1 T (43 MHz) showing the magnetic evolution of 3.1 mM of (a) $[Ir(H)_2(I)(CO)(PPh_3)_2]$ and (b) $[Ir(H)_2(I)(^{13}CO)(PPh_3)_2]$ each alongside an annotated reference 1D ^{1}H spectrum. 2D spectra are shown with a 1x scaling factor (white background) and a 10x scaling factor (grey background). Data was collected in 64 steps using d_1 = 1 s and τ delays between 0 and 31 ms, in 0.5 ms increments. Reference 1D spectra are taken from step 2 (τ = 0.5 ms) with an additional inset from step 1 (τ = 0 ms) to clearly highlight hydride peaks present at < −20 ppm. Oscillation frequencies are: $f_{2a} = (283 \pm 12)$, $f_{2b+} = (310 \pm 20)$, $f_{2b-} = (260 \pm 20)$, $f_{4+} = (350 \pm 20)$ and $f_{4-} = (210 \pm 20)$ Hz.

tion of *cis*-$[Ru(H)_2(dppe)_2]$, $[Ir(H)_2(I)(CO)(PPh_3)_2]$. and $[Ir(H)_2(I)(^{13}CO)(PPh_3)_2]$. For *cis*-$[Ru(H)_2(dppe)_2]$, the high efficiency of our approach allowed observation of zero-quantum oscillations of the pH_2-derived hydride ligands during the pump-probe delay. These results proved directly comparable to those reported with laser-initiation at 600 MHz using far more expensive hardware.[60] The high-intensity peak at 0 Hz observed in the benchtop pump-probe NMR spectrum arises from imperfect preservation of the pH_2 singlet by the spin-lock during UV irradiation.

Photochemical pump, benchtop NMR probe spectra mapping H_2 addition to *trans*-$[IrI(CO)(PPh_3)_2]$ and *trans*-$[IrI(^{13}CO)(PPh_3)_2]$ were again of good quality. The resultant spectra contained zero-quantum correlations for the products $[Ir(H)_2(I)(CO)(PPh_3)_2]$ and $[Ir(H)_2(I)(^{13}CO)(PPh_3)_2]$ that arise from the differences in chemical shift and heteronuclear J couplings between the pH_2-derived hydride ligands in the two complexes. In addition to the expected correlations, zero-quantum oscillations were also observed for the light-induced ligand exchange product $[Ir(H)_2(I)(PPh_3)_3]$. Additional hyperpolarised hydride ligand peaks were assigned to an iridium dimer, which did not exhibit zero-quantum oscillations, indicating that incoherent thermal exchange of pH_2 occurs during the pump-probe delay. These two very low-concentration photo-products are only observable in these 1 T benchtop NMR spectra due to the significant signal enhancements afforded by pH_2, and the synchronisation of the UV irradiation and NMR detection.

In terms of the general applicability of this method, a wide range of metal complexes undergo photochemically initiated loss of a two-electron donor ligand, following which dihydrogen can rapidly add to the resulting photoproduct. Complexes of the second and third transition metal series are particularly well-suited for this approach, as they are most likely to follow the required diamagnetic reaction pathway.[72] Here we have focused on ^{1}H detection; however, the method can be expanded to observe hyperpolarisation of heteronuclei such as ^{31}P.[55] This could be achieved through pulse sequence modification[73] or magnetic field cycling.[74,75]

There are several areas through which the experimental design established within this paper could be furthered. For example, extending the pump-probe method to observe chemical evolution on millisecond to second timescales could be explored through pulse-

sequence design, for example by applying a spoiler pulse at the end of the UV irradiation period to destroy any pre-existing hyperpolarised signal.[76,77] Alternatively, switching the light source to a laser would provide a synchronous starting point at the cost of increasing the complexity and expense of the system. Improvements could also be made through the incorporation of automated *in situ* bubbling of pH_2 through the sample to remove the need to manually refresh the pH_2 within the sample during experiments.

CRediT authorship contribution statement

Alastair Robinson: Methodology, Software, Formal Analysis, Investigation, Writing - Original Draft, Visualisation, Writing - Review and Editing **Fraser Hill-Casey:** Methodology, Resources. **Simon Duckett:** Conceptualization, Writing - Review and Editing, Supervision, Project Administration, Funding Acquisition. **Meghan Halse:** Conceptualisation, Formal Analysis, Writing - Review and Editing, Supervision, Project Administration, Funding Acquisition.

Acknowledgements

Financial support from the University of York (A.D.R. studentship) and Engineering and Physical Sciences Research Council (EPSRC) UK (EP/R028745/1 and EP/M020983/1) is gratefully acknowledged. The authors would also like to thank Dr. Jenny Lewis, Dr. Adam Gaunt and Dr. Arnaud Comment for loaning the Bluewave 75 lamp used in this research. A further thank you is extended to Dr. Peter Rayner and Dr. Victoria Annis for their assistance in the synthesis of the metal complexes used in this work. For the purpose of open access, the author has applied a Creative Commons Attribution (CC BY) licence to any Author Accepted Manuscript version arising from this submission. The data supporting this research is openly available for download from the York Research Database at DOI:xxxxx

Conflict of interest

We have no conflicts of interest to declare.

Supporting Information

Additional details on the optimisation of the instrumentation and the communication between the UV lamp and the NMR spectrometer, can be found online in the Supporting Information document. References to the relevant sections of the Supporting Information have been provided in the text.

Table of contents graphic

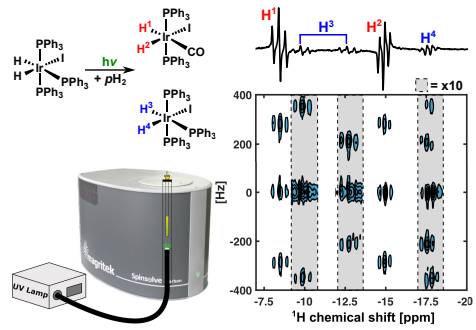

In situ monitoring of photochemical ligand exchange and oxidative addition using a benchtop NMR spectrometer, equipped with through-bore UV irradiation and *para*hydrogen hyperpolarisation, is presented. The method is applied to a range of iridium complexes, effectively mapping two photochemical pathways and enabling the identification of several ligand-exchange products.

References

[1] M. V. Silva Elipe, *Anal. Chim. Acta* **2003**, *497*, 1.

[2] U. Holzgrabe, R. Deubner, C. Schollmayer, B. Waibel, *J. Pharm. Biomed.* **2005**, *38*, 806.

[3] T. Maschmeyer, L. P. Yunker, J. E. Hein, *React. Chem. Eng.* **2022**, *7*, 1061.

[4] M. P. Johnson, *Essays Biochem.* **2016**, *60*, 255.

[5] M. Boggio-Pasqua, C. F. Burmeister, M. A. Robb, G. Groenhof, *Phys. Chem. Chem. Phys.* **2012**, *14*, 7912.

[6] D. Phillips, *Photochem. Photobiol. Sci.* **2010**, *9*, 1589.

[7] K. Plaetzer, B. Krammer, J. Berlanda, F. Berr, T. Kiesslich, *Lasers Med. Sci.* **2009**, *24*, 259.

[8] M. Fischer, *Angew. Chem., Int. Ed. Engl.* **1978**, *17*, 16.

[9] L. Buglioni, F. Raymenants, A. Slattery, S. D. Zondag, T. Noël, *Chem. Rev.* **2021**, *122*, 2752.

[10] G. E. Ball, *Spectrosc. Prop. Inorg. Organomet. Compd.* **2010**, *41*, 262.

[11] C. Wolff, J. Kind, H. Schenderlein, H. Bartling, C. Feldmeier, R. M. Gschwind, M. Biesalski, C. M. Thiele, *Magn. Reson. Chem.* **2016**, *54*, 485.

[12] B. Procacci, S. S. Roy, P. Norcott, N. Turner, S. B. Duckett, *J. Am. Chem. Soc.* **2018**, *140*, 16855.

[13] L. Bliumkin, R. Dutta Majumdar, R. Soong, A. Adamo, J. P. D. Abbatt, R. Zhao, E. Reiner, A. J. Simpson, *Environ. Sci. Technol.* **2016**, *50*, 5506.

[14] A. M. R. Hall, R. Broomfield-Tagg, M. Camilleri, D. R. Carbery, A. Codina, D. T. E. Whittaker, S. Coombes, J. P. Lowe, U. Hintermair, *Chem. Commun.* **2018**, *54*, 30.

[15] R. Kaptein, K. Dijkstra, K. Nicolay, *Nature* **1978**, *274*, 293.

[16] J. Hore, R. W. Broadhurst, *Prog. Nucl. Magn. Reson. Spectrosc.* **1993**, *25*, 345.

[17] B. Koeppe, P. M. Tolstoy, H. H. Limbach, *J. Am. Chem. Soc.* **2011**, *133*, 7897.

[18] P. M. Tolstoy, B. Koeppe, G. S. Denisov, H. H. Limbach, *Angew. Chem.* **2009**, *48*, 5745.

[19] R. Kaptein, *Biol. Magn. Reson.* **1982**, *4*, 145.

[20] S. B. Duckett, M. W. George, O. S. Jina, S. L. Matthews, R. N. Perutz, X. Z. Sun, K. Q. Vuong, *Chem. Commun.* **2009**, pages 1401–1403.

[21] E. Stadler, M. Dommaschk, P. Frühwirt, R. Herges, G. Gescheidt, *ChemPhysChem* **2018**, *19*, 571.

[22] C. L. Lerman, M. Cohn, *Biochem. Biophys. Res. Commun.* **1980**, *97*, 121.

[23] I. Kuprov, P. J. Hore, *J. Magn. Reson.* **2004**, *171*, 171.

[24] Y. Ji, D. A. DiRocco, J. Kind, C. M. Thiele, R. M. Gschwind, M. Reibarkh, *ChemPhotoChem* **2019**, *3*, 984.

[25] E. E. Brown, I. Mandzhieva, P. M. Tomhon, T. Theis, F. N. Castellano, *ACS Cent. Sci.* **2022**, *8*, 1548.

[26] J. E. Bramham, A. P. Golovanov, *Commun. Chem.* **2022**, *5*, 1.

[27] K. Singh, B. Blümich, *Trends. Anal. Chem.* **2016**, *83*, 12.

[28] H. Kim, Y. Yonekura, J. I. Yoshida, *Angew. Chem. Int. Ed.* **2018**, *57*, 4063.

[29] M. Goldbach, E. Danieli, J. Perlo, B. Kaptein, V. M. Litvinov, B. Blümich, F. Casanova, A. L. Duchateau, *Tetrahedron Lett.* **2016**, *57*, 122.

[30] M. V. Silva Elipe, R. R. Milburn, *Magn. Reson. Chem.* **2016**, *54*, 437.

[31] S. T. Knox, S. Parkinson, R. Stone, N. J. Warren, *Polym. Chem.* **2019**, *10*, 4774.

[32] M. Leutzsch, A. J. Sederman, L. F. Gladden, M. D. Mantle, *Magn. Reson. Imaging* **2019**, *56*, 138.

[33] E. Danieli, . J. Perlo, . A. L. L. Duchateau, G. K. M. Verzijl, V. M. Litvinov, . B. Blümich, F. Casanova, *ChemPhysChem.* **2014**, *15*, 3060 .

[34] S. K. Küster, E. Danieli, B. Blümich, F. Casanova, *Phys. Chem. Chem. Phys.* **2011**, *13*, 13172.

[35] B. Blümich, G. K. M. Verzijl, V. M. Litvinov, E. Danieli, F. Casanova, A. L. L. Duchateau, J. Perlo, A. L. L. Duchateau, G. K. M. Verzijl, V. M. Litvinov, B. Blümich, F. Casanova, *ChemPhysChem* **2014**, *15*, 3060.

[36] M. V. Gomez, A. De La Hoz, *Beilstein J. Org. Chem.* **2017**, *13*, 285.

[37] P. Giraudeau, F. X. Felpin, *React. Chem. Eng.* **2018**, *3*, 399.

[38] R. Sakla, D. A. Jose, *Inorganica Chim. Acta* **2021**, *516*, 120134.

[39] M. W. Dale, D. J. Cheney, C. Vallotto, C. J. Wedge, *Phys. Chem. Chem. Phys* **2020**, *22*, 28173.

[40] J. Bernarding, C. Bruns, I. Prediger, M. Plaumann, *Appl. Magn. Reson.* **2022**, *53*, 1375.

[41] A. I. Silva Terra, D. A. Taylor, M. E. Halse, *Prog. Nucl. Magn. Reson. Spectrosc.* **2024**, *144-145*, 153.

[42] J. Eills, D. Budker, S. Cavagnero, E. Y. Chekmenev, S. J. Elliott, S. Jannin, A. Lesage, J. Matysik, T. Meersmann, T. Prisner, J. A. Reimer, H. Yang, I. V. Koptyug, *Chem. Rev.* **2023**, *123*, 1417.

[43] C. R. Bowers, D. P. Weitekamp, *Phys. Rev. Lett.* **1986**, *57*, 2645.

[44] C. R. Bowers, D. P. Weitekamp, *J. Am. Chem. Soc.* **1987**, *109*, 5541.

[45] T. C. Eisenschmid, R. U. Kirss, P. P. Deutsch, S. I. Hommeltoft, R. Eisenberg, J. Bargon, R. G. Lawler, A. L. Balch, *J. Am. Chem. Soc.* **1987**, *109*, 8089.

[46] M. E. Halse, *Trends Anal. Chem.* **2016**, *83*, 76.

[47] R. A. Green, R. W. Adams, S. B. Duckett, R. E. Mewis, D. C. Williamson, G. G. Green, *Prog. Nucl. Magn. Reson. Spectrosc.* **2012**, *67*, 1.

[48] J. Natterer, J. Bargon, *Prog. Nucl. Magn. Reson. Spectrosc.* **1997**, *31*, 293.

[49] R. Kaptein, K. Dijkstra, F. Müller, C. G. Van Schagen, A. J. Visser, *J. Magn. Reson.* **1978**, *31*, 171.

[50] P. Hore, E. Zuiderweg, R. Kaptein, K. Dijkstra, *Chem. Phys. Lett.* **1981**, *83*, 376.

[51] R. J. Miller, G. L. Closs, *Rev. Sci. Instrum.* **1981**, *52*, 1876.

[52] F. Torres, M. Bütikofer, G. R. Stadler, A. Renn, H. Kadavath, R. Bobrovs, K. Jaudzems, R. Riek, *J. Am.Chem. Soc.* **2023**, *145*, 12066.

[53] G. R. Stadler, T. F. Segawa, M. Bütikofer, V. Decker, S. Loss, B. Czarniecki, F. Torres, R. Riek, *Angew. Chem. Int. Ed.* **2023**, *62*, e20230869.

[54] C. Godard, P. Callaghan, J. L. Cunningham, S. B. Duckett, J. A. B. Lohman, R. N. Perutz, *Chem. Commun.* **2002**, pages 2836–2837.

[55] O. Torres, B. Procacci, M. E. Halse, R. W. Adams, D. Blazina, S. B. Duckett, B. Eguillor, R. A. Green, R. N. Perutz, D. C. Williamson, *J. Am. Chem. Soc.* **2014**, *136*, 10124.

[56] A. N. Pravdivtsev, A. V. Yurkovskaya, P. A. Petrov, H.-M. Vieth, *Phys. Chem. Chem. Phys.* **2017**, *19*, 25961.

[57] A. S. Kiryutin, V. P. Kozinenko, A. V. Yurkovskaya, *ChemPhotoChem* **2024**, *8*, e202300151.

[58] B. Procacci, P. M. Aguiar, M. E. Halse, R. N. Perutz, S. B. Duckett, *Chem. Sci.* **2016**, *7*, 7087.

[59] B. Procacci, S. B. Duckett, M. W. George, M. W. Hanson-Heine, R. Horvath, R. N. Perutz, X. Z. Sun, K. Q. Vuong, J. A. Welch, *Organometallics* **2018**, *37*, 855.

[60] M. E. Halse, B. Procacci, S. L. Henshaw, R. N. Perutz, S. B. Duckett, *J. Magn. Reson.* **2017**, *278*, 25.

[61] A. D. Robinson, F. Hill-Casey, S. B. Duckett, M. E. Halse, *Phys. Chem. Chem. Phys.* **2024**, *26*, 14317.

[62] P. B. Chock, J. Halpern, *J. Am. Chem. Soc* **1966**, *88*, 3511.

[63] M. J. Burk, R. H. Crabtree, *Inorg. Chem.* **1986**, *25*, 931.

[64] S. P. Nolan, T. S. R. Belderrain, R. H. Grubbs, *Organometallics* **1997**, *16*, 5569.

[65] R. Shaver, S. Van Wallendael, D. P. Rillema, *J. Chem. Educ.* **1991**, *68*, 604.

[66] P. M. Richardson, R. O. John, A. J. Parrott, P. J. Rayner, W. Iali, A. Nordon, M. E. Halse, S. B. Duckett, *Phys. Chem. Chem. Phys.* **2018**, *20*, 26362.

[67] P. B. Chock, J. Halpern, *J. Am. Chem. Soc.* **1966**, *88*, 3511.

[68] D. Blazina, S. B. Duckett, T. K. Halstead, C. M. Kozak, R. J. K. Taylor, M. S. Anwar, J. A. Jones, H. A. Carteret, *Magn. Reson. Chem.* **2005**, *43*, 200.

[69] M. Carravetta, M. H. Levitt, *J. Am. Chem. Soc.* **2004**, *126*, 6228.

[70] M. H. Levitt, R. Freeman, *J. Magn. Reson.* **1981**, *43*, 502.

[71] M. H. Levitt, R. Freeman, T. Frenkiel, *J. Magn. Reson.* **1982**, *47*, 328.

[72] R. N. Perutz, B. Procacci, *Chem. Rev.* **2016**, *116*, 8506.

[73] D. T. Pegg, D. M. Doddrell, M. R. Bendall, *J. Magn. Reson.* **1983**, *51*, 264.

[74] A. Svyatova, V. P. Kozinenko, N. V. Chukanov, D. B. Burueva, E. Y. Chekmenev, Y. W. Chen, D. W. Hwang, K. V. Kovtunov, I. V. Koptyug, *Sci. Rep.* **2021**, *11*, 5646.

[75] D. B. Burueva, S. V. Sviyazov, N. V. Chukanov, N. R. Mustafin, O. G. Salnikov, E. Y. Chekmenev, K. V. Kovtunov, I. V. Koptyug, *J. Magn.Reson. Open* **2024**, *21*, 100176.

[76] B. A. Rodin, K. F. Sheberstov, A. S. Kiryutin, L. J. Brown, R. C. Brown, M. Sabba, M. H. Levitt, A. V. Yurkovskaya, K. L. Ivanov, *J. Chem. Phys.* **2019**, *151*, 234203.

[77] S. J. Elliott, O. Cala, Q. Stern, S. F. Cousin, D. Eshchenko, R. Melzi, J. G. Kempf, S. Jannin, *Phys. Chem. Chem. Phys.* **2021**, *23*, 9457.